Response to Request for Additional Information – ANP-10287P
"Incore Trip Setpoint and Transient Methodology for U.S. EPR Topical Report"
(TAC No. Q00013)

RAI-1. *Describe the implications of mixed cores in the methodology. How will multiple DNBR correlations be implemented in the protection system? How will uncertainties and parameters of the on-line DNBR model (e.g. FH and FG) be recalculated?*

Response 1:

Mixed core methodology is not being proposed for the U.S. EPR; therefore, AREVA NP is not requesting NRC review and approval of this methodology for use for mixed cores.

RAI-2. *Describe the tuning of the protection systems based on plant measurements (e.g., actual plant flow) at startup. Would a full set of Chapter 15 analysis be required if the setpoint assumptions are changed?*

Response 2:

The U.S. EPR is configured to operate on sets of flow-independent setpoints. Therefore, the setpoint calculation must be conducted considering a flow rate that results in a conservative setpoint, regardless of the operating flow rate. **[**

] These conservative setpoints also form the basis for bounding safety analysis calculations.

If an operating U.S. EPR transitions to flow-dependent monitoring or trip limits, the methodology for generating or confirming **[ ]** setpoints would require additional scope, and the manner in which safety analysis calculations would also require modification. Therefore, potential implementation of flow-dependent setpoints is not within the scope of this topical report (TR).

There are two flow-related constants in the low departure from nucleate boiling ratio (DNBR) channel limiting safety system setting (LSSS) as described in TR Section C.1.3 (TR page C-3). These are reference values for reactor coolant pump (RCP) speed (Ω_{ref}) and the volumetric flow rate (Q_{ref}), **[**

] The frequency at which these parameters will be updated is consistent

[

]

RAI-3. *A) Provide a simulation of burnup over 15 days and the change in SPND calibration constants. B) How is Cij changing with time? C) How does the change in Cij affect the setpoint?*

Response 3:

Figure RAI 3-1: Decalibration of the SPNDs Over 15 Days – DNBR

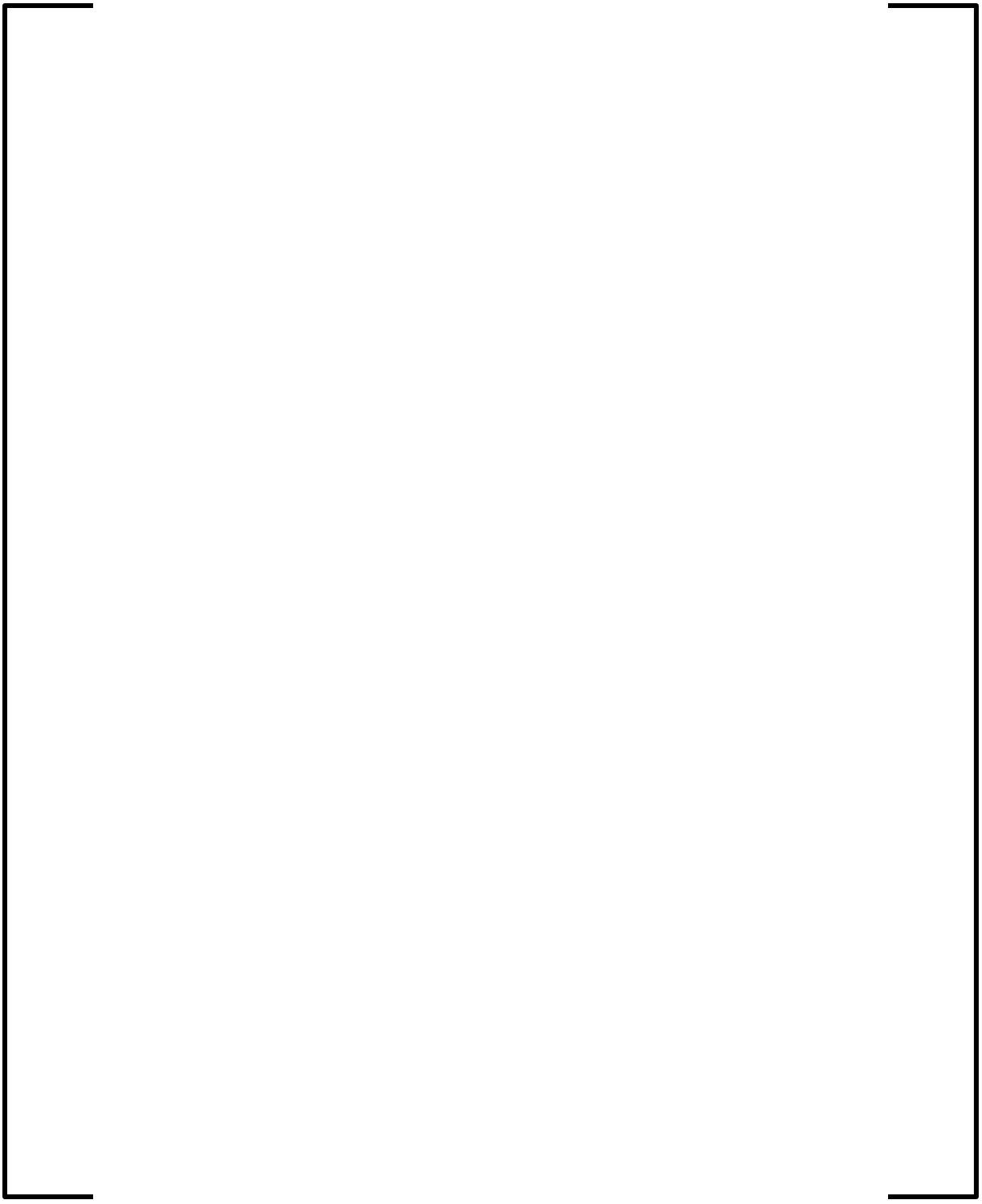

Figure RAI 3-2: Decalibration of the SPNDs Over 15 Days – LPD

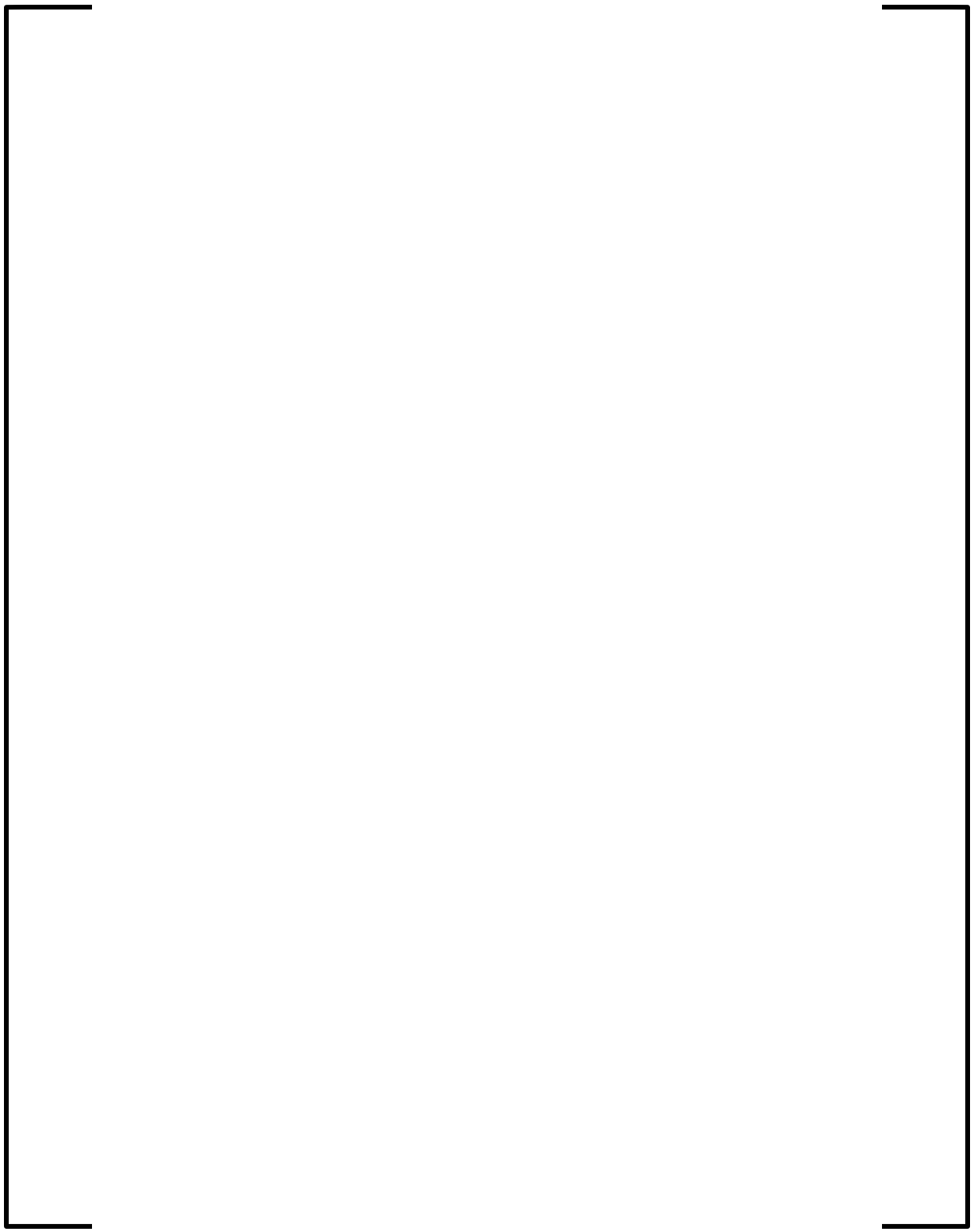

RAI-4. *Describe the reload process for setpoint calculations. Define what calculations are performed generically for each fuel type, and which are cycle-specific.*

Response 4:

The methodology in the TR supports both cycle-specific DNBR and LPD setpoints and cycle-independent setpoints. Thus, setpoint calculations are conducted every cycle to assess the impact of the core design upon the setpoints. The TR methodology evaluates the impact of changes in axial and radial power distributions achievable for a given fuel loading upon the setpoints.

When a plant uses cycle-specific setpoints, the **[ ]** setpoint calculations are rerun for a given core design to appropriately establish the Cycle N+1 setpoints. When a plant uses cycle-independent setpoints, the **[ ]** setpoint calculations are rerun for a given core design to confirm that the cycle N setpoints remain conservatively bounding for Cycle N+1. Figures RAI 4-1 and RAI 4-2 show a general process work flow for **[ ]** setpoints.

The following calculations are performed prior to each upcoming cycle, regardless of whether cycle-specific or cycle-independent setpoints are being supported:

[ ]

Further information on these calculations is provided below. Table RAI 4-1 provides a summary of the requirements of cycle-dependent or cycle-independent setpoints.

[ ]

The **[ ]** Low DNBR channel and **[ ]** high LPD channel setpoint calculations are conducted in their entirety each cycle, considering power distributions from the particular core design for the upcoming cycle, and reflecting any plant changes that potentially impact the trip intercession region[1]. This applies to the cycle-dependent and cycle-independent setpoint treatments. **[**

] In a cycle-independent treatment, the setpoints are not updated unless they are analytically invalidated.

[1] For example, if the pressurizer low pressure trip had its setpoint lowered for some reason, then a lower span of pressure could be considered in the Low DNBR Channel setpoint calculation.

[

]

Tripping in response to synthesized DNBR based upon incore power distribution measurements leads to differences in trip times relative to a pressurized water reactor (PWR) design that protects against DNBR by tripping on inferential variables like temperature or gross reactor power. [

] In contrast, for a plant tripping on inferential variables will be much more cycle-independent, [

]

[

]

Figure RAI 4-2 shows the process work flow for the **[** **]** for a follow-on cycle.

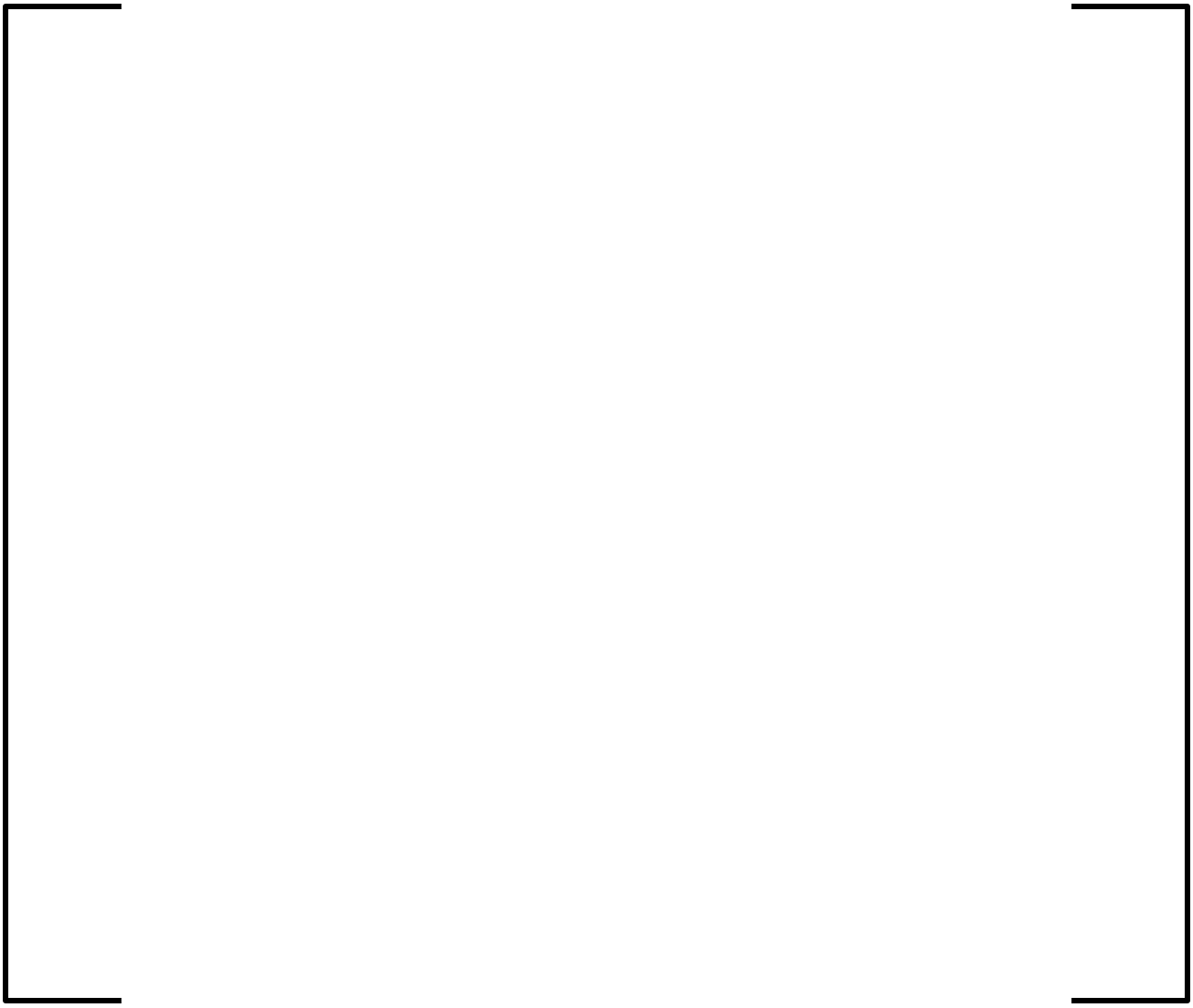

Table RAI 4-1 Summary of Setpoint Calculations for Cycle-Dependence

Figure RAI 4-1: Cycle-Specific Work Flow for Setpoints – Part I

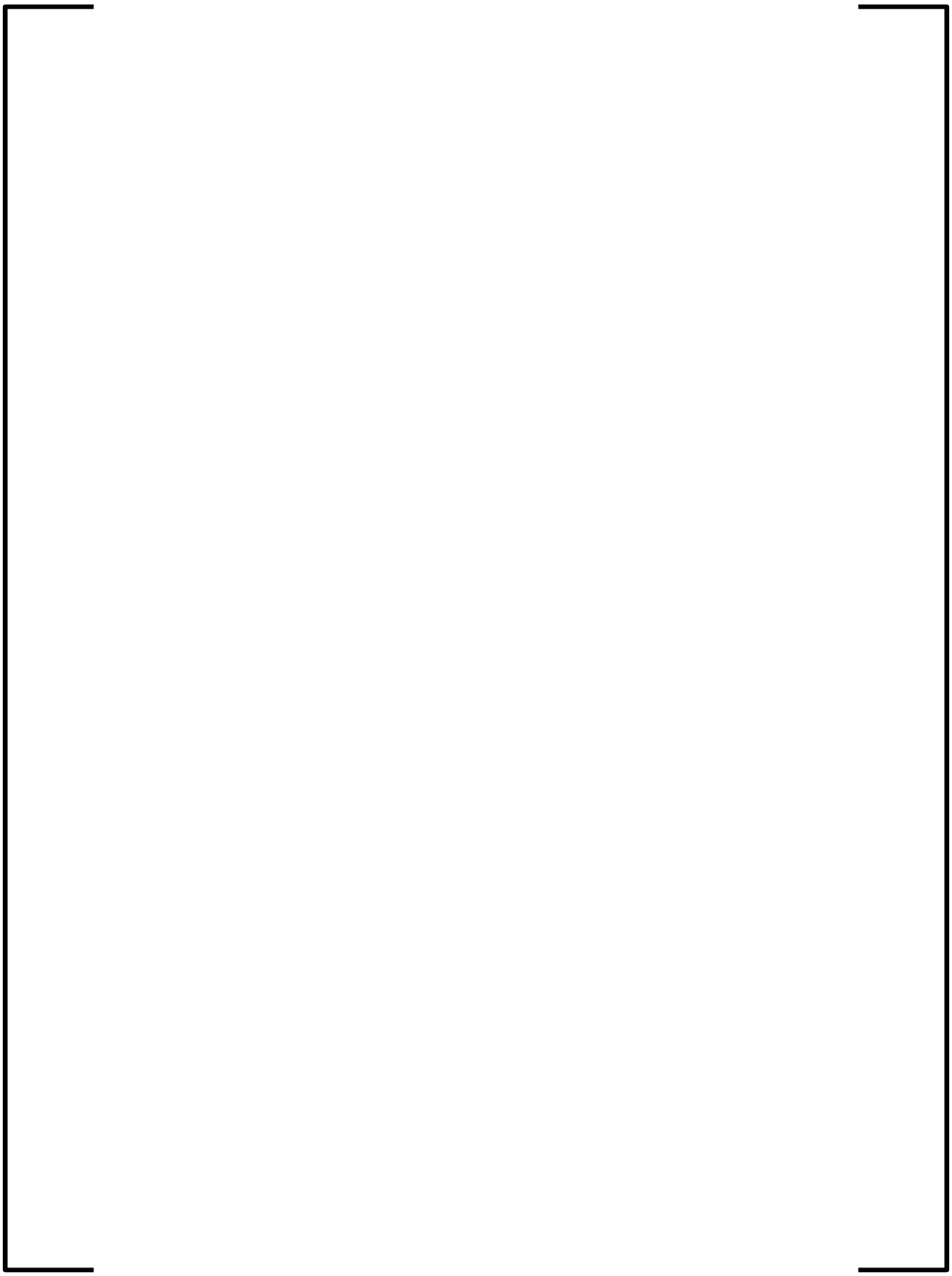

Figure RAI 4-2: Cycle-Specific Work Flow for Setpoints – Part II

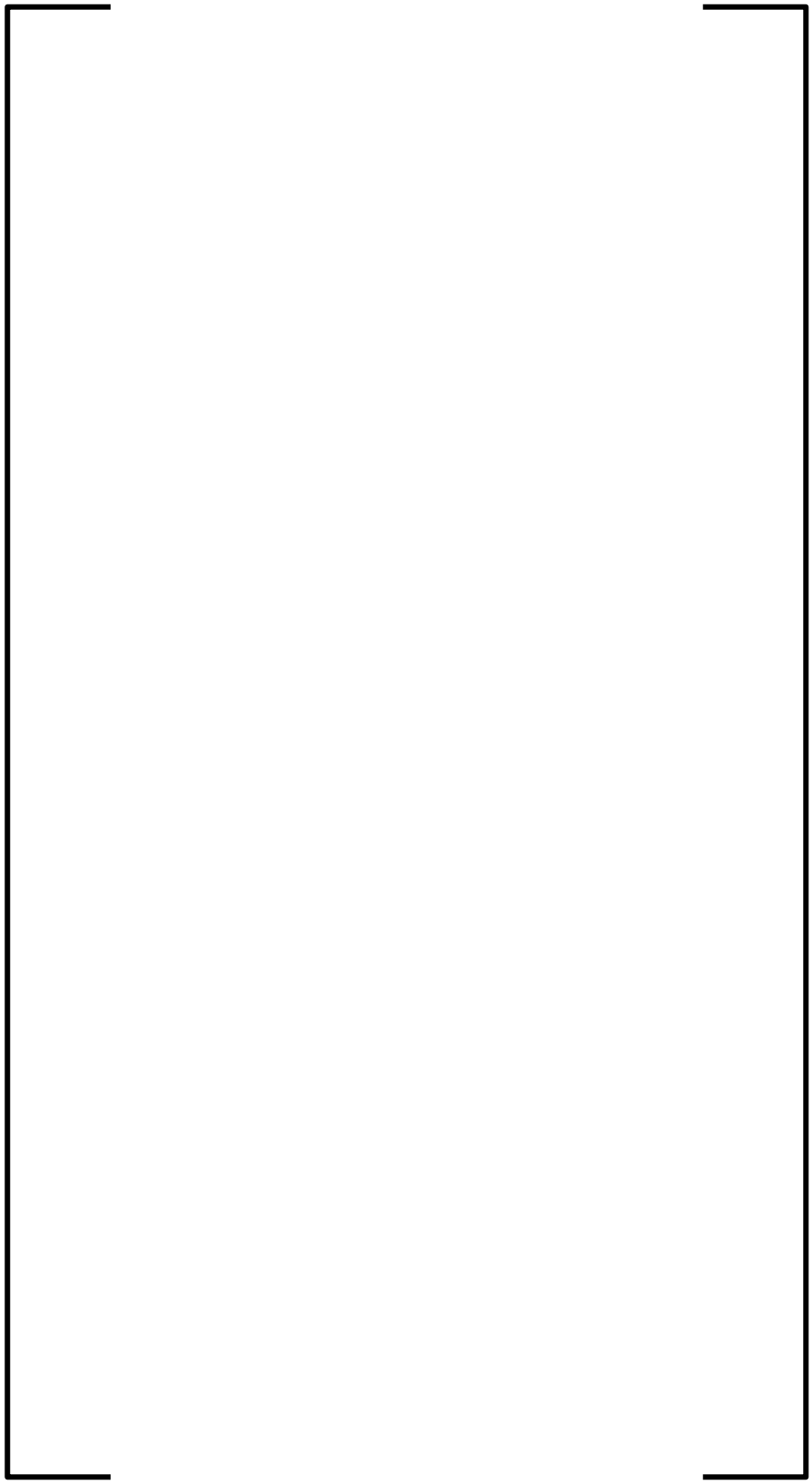

RAI-5. *Describe what setpoint values will be included in the COLR. Are any setpoints cycle independent? What are the criteria to verify the applicability of cycle-independent values?*

Response 5:

The COLR typically contains the following incore reactor trip and partial trip setpoints (notation used is the same as in TR Tables 3-2 and Table 6-2). For the setpoints below, the term 'x SPND' indicates six setpoints, each one representing zero through five SPND failures.

- Low DNBR channel LSSS - symmetric reactor trip on low DNBR ($DNBR_{RT}^{x\ SPND}$)
- Low DNBR channel LSSS - partial reactor trip on low DNBR ($DNBR_{PT}^{x\ SPND}$)
- Low DNBR channel LSSS – imbalance/(single) rod drop trip on low DNBR ($DNBR_{IMB/RD}^{x\ SPND}$)
- Low DNBR channel LSSS – (multiple) rod drop trip on low DNBR ($DNBR_{RD}^{x\ SPND}$)
- Low DNBR channel LSSS – symmetric reactor trip on high exit quality ($\chi_{RT}^{x\ SPND}$)
- Low DNBR channel LSSS – imbalance/rod drop trip on high exit quality ($\chi_{IMB/RD}^{x\ SPND}$)
- Low DNBR channel LSSS – axially-dependent imbalance thresholds for transitioning to an IMB/RD setpoint
- High LPD channel LSSS – reactor trip on High LPD ($HLPD_{RT}^{x\ SPND}$)
- High LPD channel LSSS – partial reactor trip on High LPD ($HLPD_{PT}^{x\ SPND}$)

Additionally, the COLR typically contains the following DNB and LPD LCO setpoints:

- DNB LCO 1 – DNB LCO setpoints for LCO1 threshold ($DNBR_{LCO1}^{x\ SPND}$)
- DNB LCO 2 – DNB LCO setpoints for LCO2 threshold ($DNBR_{LCO2}^{x\ SPND}$)
- Upper core half LPD LCO 1 – LPD LCO setpoints for LCO1 threshold ($HLPD\_ULCO1_{x\ SPND}$)
- Upper core half LPD LCO 2 – LPD LCO setpoints for LCO2 threshold ($HLPD\_ULCO2_{x\ SPND}$)
- Lower core half LPD LCO 1 – LPD LCO setpoints for LCO1 threshold ($HLPD\_LLCO1_{x\ SPND}$)
- Lower core half LPD LCO 2 – LPD LCO setpoints for LCO2 threshold ($HLPD\_LLCO2_{x\ SPND}$)

The process by which cycle-independent setpoint values are established is described in the response to RAI-4.

RAI-6. *Provide a description of the process used by Areva to select the database of power shapes and statepoints used for tolerance determination. Specify the typical number of shapes and statepoints that are used for the setpoint determination for a typical reload setpoint analysis.*

Response 6:

A description of the process used to select power distributions (i.e., power shapes) and statepoints is provided below.

Power Distributions

A three dimensional reactor core model is depleted in a manner consistent with the expected behavior of the core through several initial cycles and the cycle being analyzed. The results from the depletions, which contain fuel assembly exposure distributions, are stored for future analysis.

These depletion results are used in a series of calculations from which a set of generic axial power distributions based on xenon oscillations and a set of transient-specific axial power distributions are generated. The majority of the AOO events are covered by the shapes included in the generic set. Specific shapes are generated for transients that bring about significant changes in the axial and/or radial power distribution, such as the dropped Rod Cluster Control Assembly (RCCA), which would not be addressed by the generic shape set.

Generic Power Distributions

Restart calculations are performed at the beginning, middle, and end of each of the cycles analyzed where control rods are inserted into the nuclear model for an extended period, that bounds actual operational practices, and then withdrawn. The resultant xenon oscillations produce a variety of axial power distributions representative of the core burnup at which the restart was performed. Several points along this oscillation are chosen to provide a range of axial offset (AO) conditions covering expected anticipated operational occurrence (AOO) conditions. Each AO condition is used to evaluate power distributions at a variety of power levels for an all rods out (ARO) case and one or more rodded cases. The characteristics of these distributions are recorded and the shape data is then made available for use in the setpoint analysis.

Transient-Specific Power Distributions

Cycle and exposure-specific power distributions are also generated by performing restart calculations from the original core depletion. The xenon oscillation results that cover the trip basis events are summarized in TR Table 4-1 and TR Table 6-1.

[

]

Statepoints

There are statepoint inputs to the setpoint analysis for trip events and inputs to the LCO setpoints. Reactor trip calculations are performed with statepoint combinations to cover the entire range of the operating space in power, inlet temperature, and flow that are attainable in transient events that rely on the incore protection functions (Table RAI 6-1). LCO analyses are performed with normal operating condition statepoints (Table RAI 6-2). **[**

]

Table RAI 6-1: Representative Ranges of Parameters in Reactor Trip Setpoint Calculations

Variable	Range	Comment
Pressure		
Low	2005 psi	Low pressurizer pressure trip setpoint
High	2415 psia	High pressurizer pressure trip setpoint
Inlet temperature		
Low	550°F	Bounds transient overcooling AOO events
High	590°F	Bounds transient overheating AOO events
RCP speed		
Low	95%	See note 1
High	105%	See note 1
Reactor power	Varies	See note 2
Radial peaking		
Low	Varies	See note 3
High	Varies	See note 3

Note 1:

Note 2:

Note 3:

Table RAI 6-2: Representative Ranges of Parameters in LCO Setpoint Calculations

Variable	Value	Comment
RCP speed	100%	Based upon Technical Specification minimum flow rate
Pressure control band	±36 psia	Centered on target operating pressure
Temperature control band	+2°/-11°F	Centered on target operating temperature. Incorporates end-of-cycle (EOC) coastdown allowance

RAI-7. *Provide a description of the process used to simulate the system and in-core scrams for transient analysis. Specify which codes and models are used for every step. Specifically, specify when LYNXT vs the online DNBR models are used.*

Response 7:

The process for transient analyses and the associated codes and models used in each step for **[** **]** is described below.

Table RAI 7-1 summarizes the codes and models used in transient analysis.

Table RAI 7-1: Summary of codes and models for transient analyses

Code or Model	Purpose
PRISM/NEMO-K (or equivalent NRC-approved neutronics code)	[ ]
S-RELAP5 (or equivalent NRC-approved plant simulation code)	[ ]
LYNXT (or equivalent NRC-approved sub-channel code)	[ ]
[ ]	[ ]

Figure RAI 7-1: Process for Coupled Transient Analysis with Incore Trips

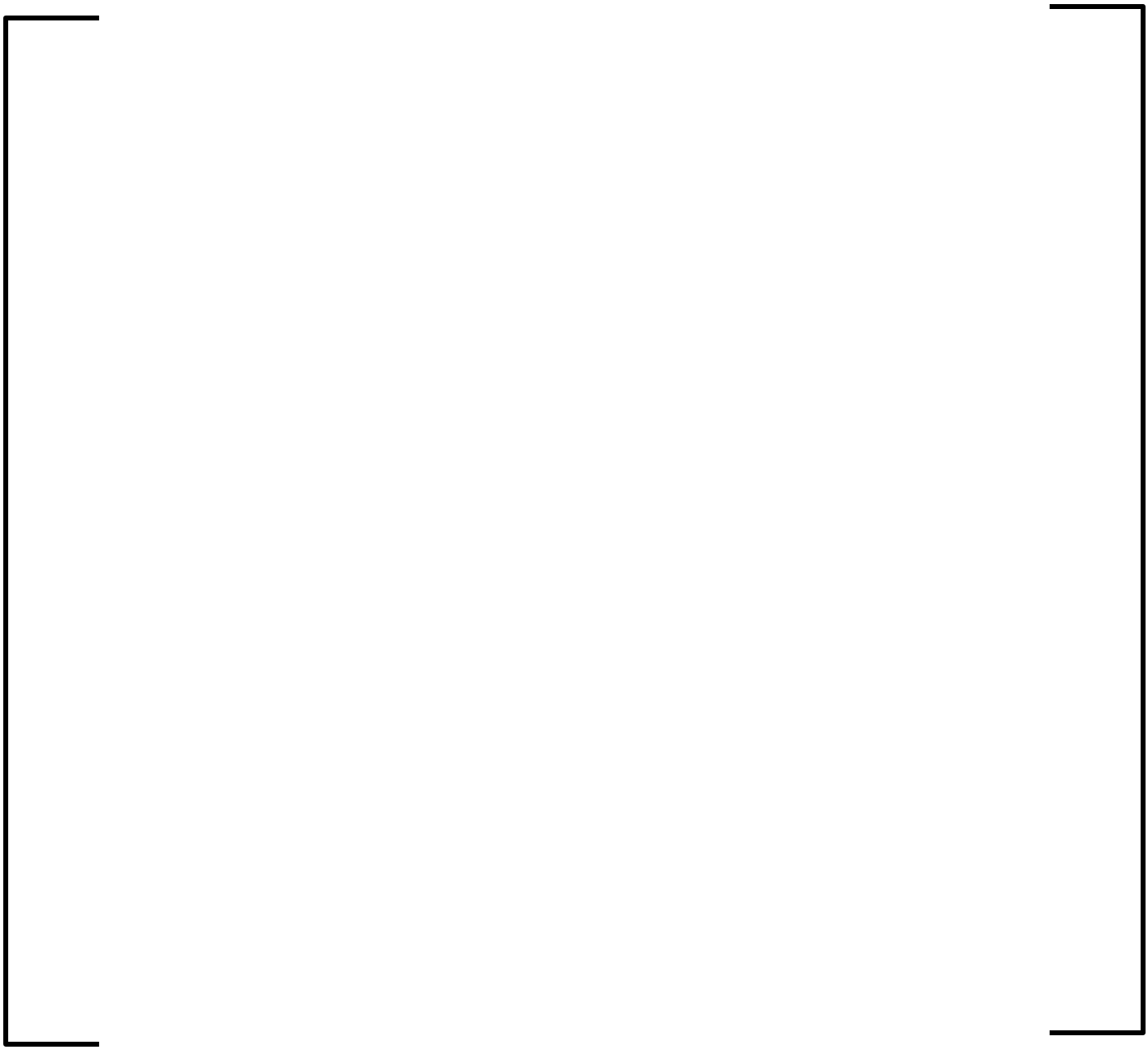

Figure RAI 7-2: Process for Decoupled Transient Analysis with Incore Trips (Part I)

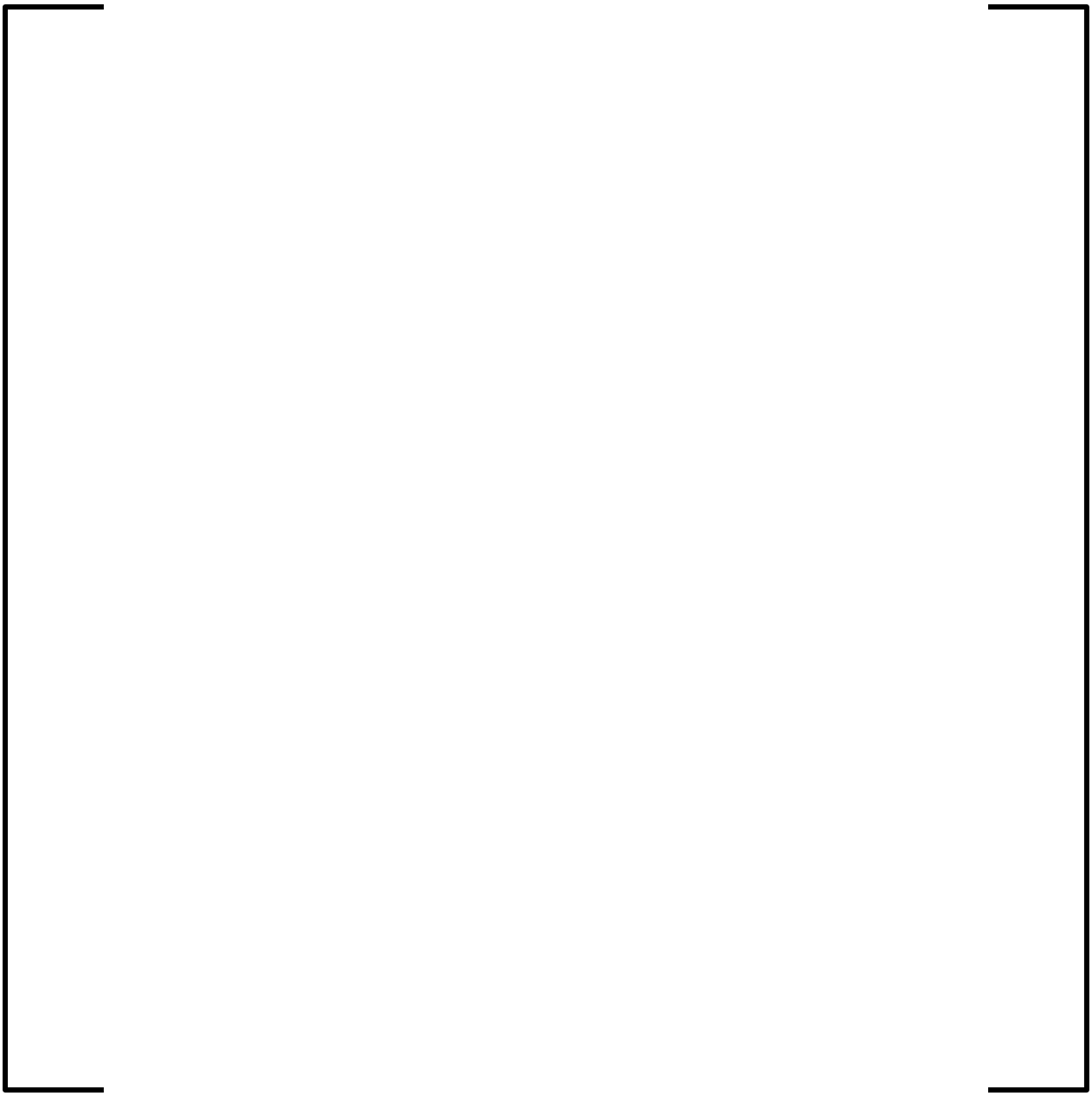

Figure RAI 7-3: Process for Decoupled Transient Analysis with Incore Trips (Part II)

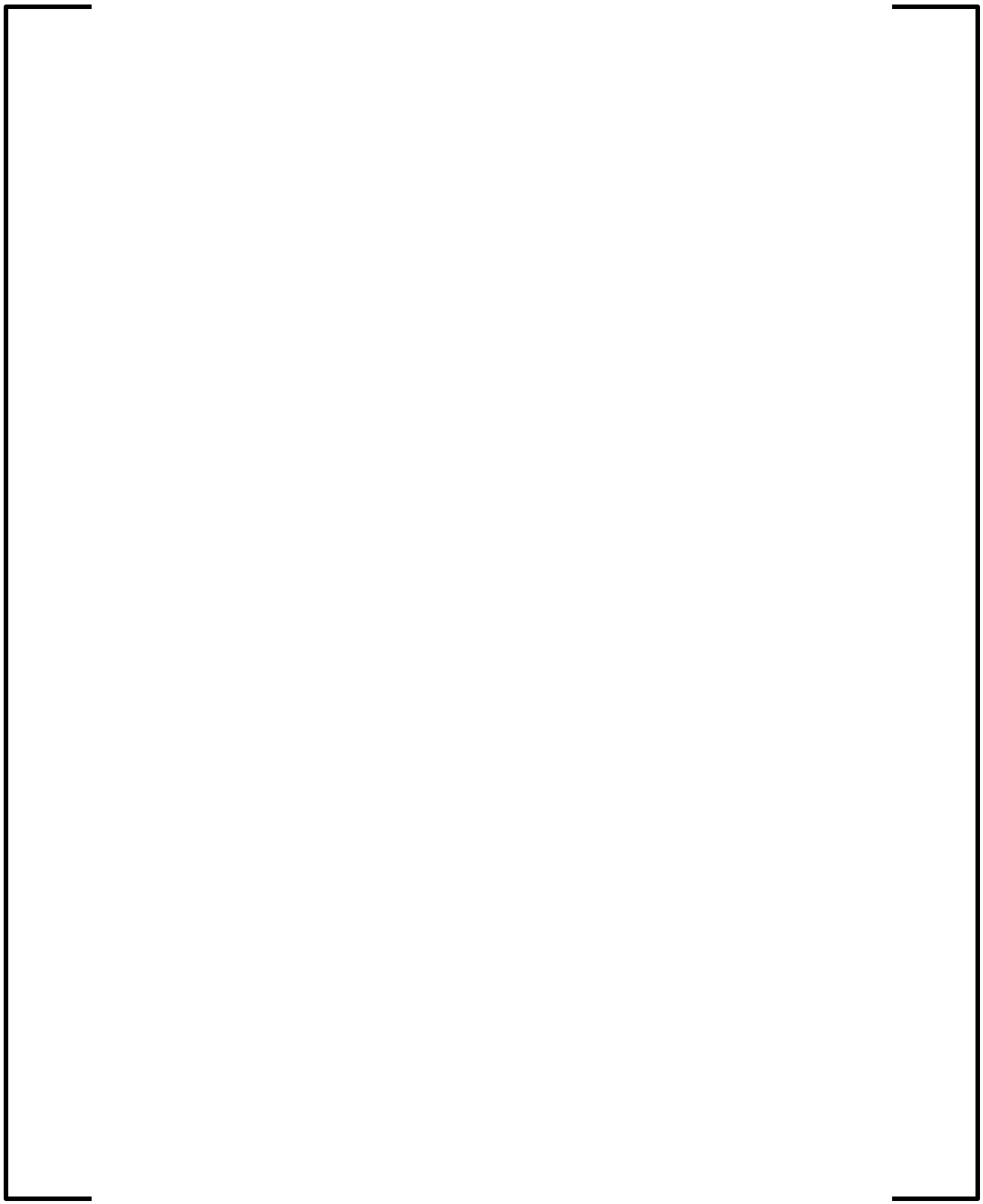

RAI-8. *A) Provide the process used to calculate the FH and FG functions for the online DNBR calculation. B) Explain what physical processes (e.g. cross flow) are being captured by these functions to make ALGO and LYNXT conditions agree. C) Since FH and FG are part of a complex setpoint, describe what process will be followed to re-set these setpoints for new fuel types. D) Describe the implications of cycle-specific load patterns (e.g., radial peaking factors)*

Response 8:

Figure RAI 8-1: Process to Generate Bias Curves

RAI-9. *Provide an example calculation of FH and FG for a representative fuel and the database of power distributions*

Response 9:

Table RAI 9-1: Representative Range of Conditions for the LYNXT Database

Figure RAI 9-1: Representative Axial Power Distributions from the LYNXT Database

Figure RAI 9-2: Representative FH Curve

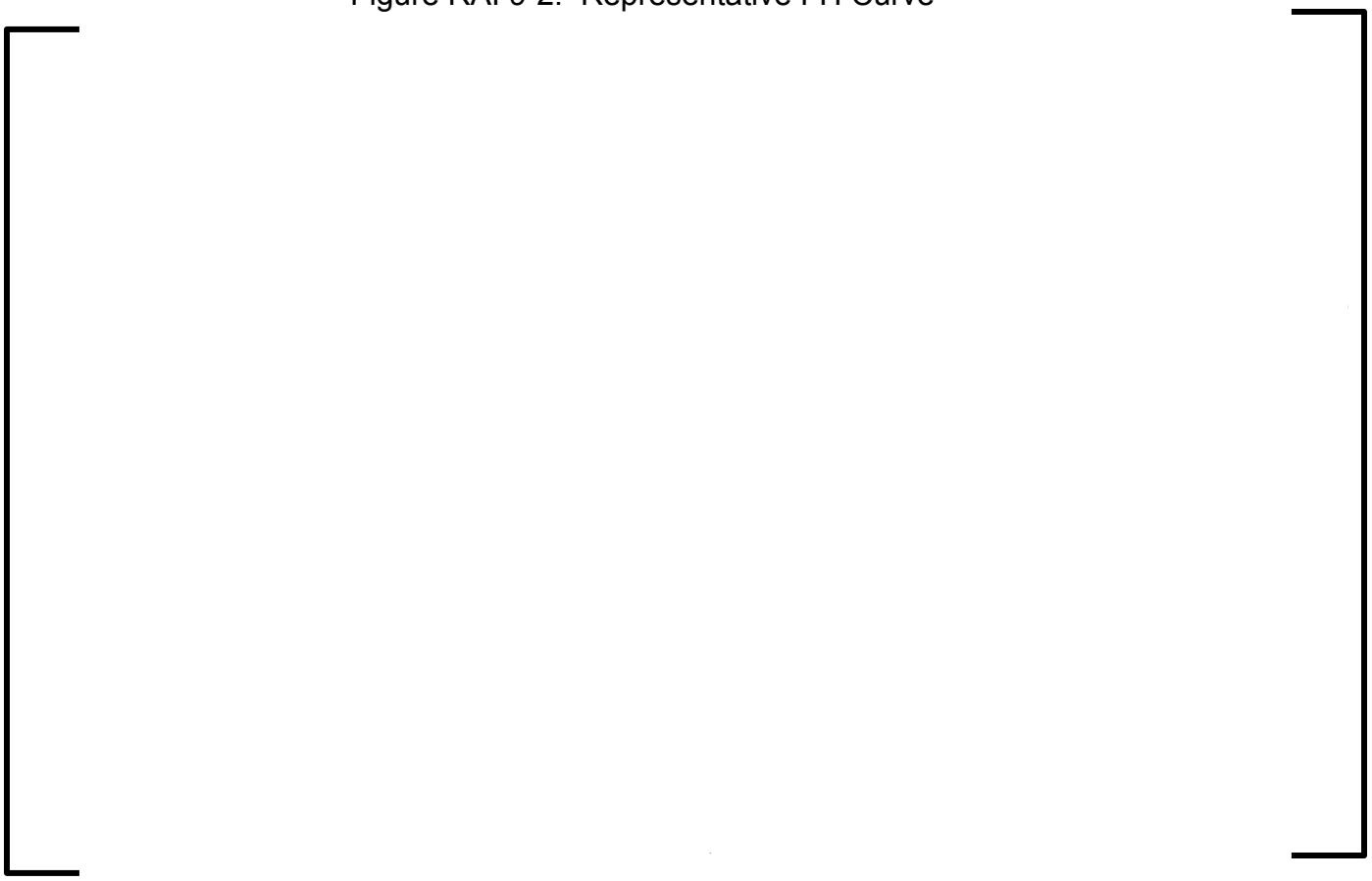

Figure RAI 9-3: Representative FG Curve.

Figure RAI 9-4: Representative Steady State Comparison of the Algorithm and LYNXT

RAI-10. *Using the Areva process for calculating FH and FG for the on-line DNBR algorithm model for new fuels, assume that the new fuel geometry is the exact geometry used for the CHF tests. Develop specific FH and FG curves and apply the on-line DNBR algorithm methodology using the CHF test operating conditions. Compare the on-line DNBR algorithm DNBR predictions against the test data.*

Response 10:

Table RAI 10-1: HTP CHF Campaigns

Table RAI 10-2: Number of CHF Tests Used in the Comparison

Table RAI 10-3: DNBR Calculated at DNB

Figure RAI 10-1: FH Bias Curve

Figure RAI 10-2: FG Bias Curve for Unit Cell

Figure RAI 10-3: FG Bias Curve for Guide Tube Cell

Figure RAI 10-4: Comparison of the Algorithm and LYNXT DNBR

RAI-11. *For a representative loss of flow event, provide the DNBR as function of time calculated by the on-line DNBR algorithm and by LYNXT. In addition, provide steady state comparisons between both codes.*

Response 11:

A representative plot of DNBR as a function of time, as calculated by the on-line DNBR algorithm and LYNXT for a four-pump loss of coolant flow event, is shown in TR Figure 10-4. LYNXT is the design subchannel code used in the generation of this plot. A steady state comparison between both codes is provided in the response to RAI-9 (see Figure RAI 9-3).

RAI-12. *Describe the isolation systems that will actuate in case an AMS tube ruptures inside the vessel.*

Response 12:

An AMS tube rupture inside the reactor pressure vessel cannot be isolated. However, portions of the AMS located within the RPV are sized (approximately 2 mm diameter) such that a break would not result in flow through the affected tube in excess of the make-up capacity of one charging pump. Furthermore, a leak in an AMS tube would be readily detected by pressure and moisture sensors, such that operators would be alerted to the leak and would take appropriate actions.

RAI-13. *Describe in physical terms the MEDIAN methodology used to extrapolate the adjusted fluxes to the non-measured nodes (Section E4 of ANP-10287). Provide an example calculation with the actual numbers for an AMS measurement.*

Response 13:

The MEDIAN methodology uses the PRISM diffusion solution method. Wherever a measurement exists, the 2 group fluxes which yield the measured activation rate can be considered as a fixed source and these measured locations are not solved for iteratively in the MEDIAN solution.

The following steps describe the process for determining the extrapolated fluxes:

[ ]

Example Calculation

As an example of the application of the MEDIAN methodology, GKN1 Cycle 26 Map 32 (cycle burnup = 1.66 GWd/MTU) will be used. Figure RAI 13-1 presents the calculated versus measured 2D F_{dh} results for this map.

For this map, location F11 is an instrumented location. In addition to the MEDIAN calculation which generated the data in Figure RAI 13-1, an additional MEDIAN calculation was performed where the measured data for location F11 was removed (i.e., the location F11 distribution is generated using the MEDIAN extrapolation methodology). As a result of these 2 sets of calculations the following F_{dh} pin axial distributions for location F11 are available:

- PRISM theoretical distribution
- MEDIAN extrapolated distribution without grid factors applied
- MEDIAN extrapolated distribution with grid factors applied
- Measured distribution (generated with the measured data in location F11 present)

Table RAI 13-1 and Figure RAI 13-2 summarize the results obtained from these calculations.

Table RAI 13-1: GKN1 Cycle 26 Map 32 Assembly F11 F_{dh} Pin Axial Values

	midpt	GKN1 Cycle 26 Map 32 Assembly F11 Fdh Values			
node	cm	calculated	inferred no grid	inferred w grid	measured
1	9.950	0.8744	0.8559	0.8696	0.8843
2	22.500	1.2513	1.2274	1.2436	1.1822
3	27.535	1.3524	1.3302	1.3442	1.3118
4	34.965	1.4694	1.4512	1.4141	1.4499
5	44.955	1.5766	1.5665	1.5353	1.5324
6	54.945	1.6500	1.6499	1.6690	1.6908
7	64.935	1.7023	1.7102	1.7336	1.7511
8	74.925	1.7367	1.7480	1.7701	1.7871
9	84.915	1.7609	1.7724	1.7754	1.7851
10	94.905	1.7790	1.7929	1.7102	1.7206
11	104.895	1.7935	1.8132	1.8292	1.8633
12	114.885	1.8036	1.8287	1.8531	1.8568
13	124.875	1.8104	1.8360	1.8606	1.8495
14	134.865	1.8160	1.8377	1.8547	1.8516
15	144.855	1.8181	1.8358	1.7534	1.7732
16	154.845	1.8171	1.8341	1.8341	1.8208
17	164.835	1.8149	1.8326	1.8555	1.8471
18	174.825	1.8086	1.8243	1.8492	1.8080
19	184.815	1.7980	1.8102	1.8313	1.8088
20	194.805	1.7849	1.7954	1.7659	1.7805
21	204.795	1.7645	1.7762	1.7238	1.7585
22	214.785	1.7363	1.7511	1.7703	1.7598
23	224.775	1.7015	1.7196	1.7430	1.7376
24	234.765	1.6490	1.6699	1.6914	1.6682
25	244.755	1.5775	1.6019	1.6099	1.5850
26	254.745	1.4838	1.5163	1.4437	1.4516
27	264.670	1.3503	1.3956	1.4066	1.3703
28	274.660	1.1632	1.2213	1.2388	1.1791
29	283.960	0.9085	0.9746	0.9904	0.9069
30	293.950	0.6024	0.6617	0.6729	0.6903

Figure RAI 13-1: GKN1 Cycle 26 Map 32 Calculated vs. Measured F_{dh} Distribution

	1	2	3	4	5	6	7	8	9	10	11	12	13	14	15
P						0.580 0.576 0.6	0.658 0.653 0.6	0.690 0.686 0.6	0.655 0.652 0.6	**0.586** **0.585** **0.2**					
O				0.646 0.643 0.5	0.822 0.817 0.6	1.392 1.382 0.7	1.585 1.574 0.7	1.555 1.544 0.7	**1.574** **1.564** **0.7**	1.376 1.366 0.8	0.810 0.802 1.0	0.631 0.623 1.2	Calculated Fdh Measured Fdh % Difference (C-M)		
N			0.779 0.775 0.5	1.505 1.498 0.5	1.598 1.589 0.6	1.066 1.060 0.6	1.431 1.421 0.7	1.063 1.055 0.7	1.411 1.399 0.8	1.047 1.034 1.3	1.553 1.527 1.7	1.485 1.465 1.4	0.778 0.770 1.2		
M		0.631 0.628 0.5	**1.485** **1.475** **0.6**	1.271 1.266 0.4	1.375 1.368 0.5	1.550 1.540 0.6	**1.083** **1.076** **0.6**	1.549 1.536 0.9	1.078 1.067 1.0	1.540 1.521 1.2	**1.357** **1.334** **1.7**	1.271 1.256 1.2	1.505 1.488 1.1	0.646 0.641 0.8	
L		0.810 0.807 0.4	1.553 1.549 0.3	**1.358** **1.366** **-0.6**	1.135 1.127 0.7	1.554 1.543 0.7	1.217 1.209 0.7	0.969 0.962 0.8	1.215 1.205 0.9	1.556 1.542 1.0	1.135 1.125 0.9	1.375 1.363 0.9	1.598 1.581 1.1	0.822 0.818 0.4	
K	0.586 0.583 0.5	1.376 1.369 0.5	1.047 1.045 0.2	1.540 1.535 0.4	**1.557** **1.543** **0.9**	1.543 1.530 0.9	1.018 1.010 0.8	1.507 1.495 0.8	1.023 1.015 0.8	1.543 1.530 0.8	1.554 1.541 0.8	1.549 1.538 0.8	**1.065** **1.056** **0.8**	1.391 1.398 -0.5	0.580 0.586 -1.0
J	0.655 0.651 0.6	1.575 1.565 0.6	1.411 1.402 0.7	1.078 1.071 0.6	1.216 1.205 0.9	**1.023** **1.013** **1.0**	1.168 1.157 0.9	1.192 1.183 0.7	1.168 1.160 0.7	1.018 1.012 0.5	1.217 1.212 0.4	1.083 1.079 0.3	1.431 1.443 -0.8	**1.585** **1.613** **-1.7**	0.658 0.666 -1.3
H	0.690 0.686 0.6	1.555 1.546 0.6	1.063 1.055 0.8	1.550 1.536 0.9	0.969 0.961 0.9	1.506 1.493 0.9	1.190 1.182 0.7	0.829 0.823 0.7	1.189 1.184 0.4	1.505 1.497 0.5	0.969 0.970 -0.2	1.549 1.554 -0.3	1.063 1.072 -0.9	1.555 1.571 -1.0	**0.690** **0.696** **-0.8**
G	0.658 0.654 0.5	**1.585** **1.581** **0.3**	1.431 1.419 0.8	1.082 1.073 0.9	1.217 1.207 0.8	1.018 1.012 0.5	1.165 1.162 0.3	1.187 1.187 0.1	1.166 1.163 0.2	**1.023** **1.025** **-0.2**	1.215 1.221 -0.5	1.078 1.087 -0.9	1.411 1.425 -1.0	1.574 1.591 -1.1	0.655 0.662 -1.1
F	0.580 0.575 0.9	1.391 1.374 1.3	**1.065** **1.049** **1.6**	1.549 1.533 1.0	1.553 1.545 0.5	1.542 1.537 0.3	1.023 1.023 0.0	1.504 1.506 -0.1	1.018 1.028 -1.0	1.542 1.555 -0.8	**1.556** **1.569** **-0.8**	1.540 1.561 -1.4	1.047 1.067 -1.9	1.376 1.395 -1.4	0.586 0.594 -1.4
E		0.821 0.809 1.5	1.598 1.578 1.2	1.375 1.360 1.1	1.134 1.130 0.4	1.556 1.553 0.2	1.215 1.218 -0.2	0.969 0.979 -1.0	1.217 1.237 -1.6	1.553 1.572 -1.2	1.135 1.147 -1.1	**1.357** **1.389** **-2.3**	1.553 1.590 -2.4	0.810 0.826 -2.0	
D		0.645 0.639 1.1	1.504 1.490 0.9	1.270 1.262 0.6	**1.357** **1.361** **-0.3**	1.539 1.542 -0.2	1.078 1.083 -0.5	1.549 1.566 -1.1	**1.083** **1.110** **-2.5**	1.549 1.578 -1.8	1.375 1.404 -2.1	1.270 1.303 -2.5	**1.485** **1.543** **-3.8**	0.631 0.651 -3.0	
C			0.778 0.775 0.4	1.484 1.482 0.2	1.553 1.552 0.1	1.047 1.051 -0.4	1.411 1.425 -1.0	**1.063** **1.073** **-0.9**	1.431 1.452 -1.4	1.066 1.088 -2.0	1.598 1.632 -2.1	1.505 1.542 -2.4	0.779 0.804 -3.1		
B				0.631 0.633 -0.3	0.810 0.817 -0.9	1.376 1.396 -1.5	**1.575** **1.601** **-1.6**	1.555 1.572 -1.1	1.585 1.609 -1.5	1.392 1.416 -1.7	0.821 0.838 -2.0	0.646 0.661 -2.3			
A						**0.586** **0.602** **-2.7**	0.655 0.667 -1.8	0.690 0.700 -1.5	0.658 0.668 -1.6	0.580 0.590 -1.7					

***BOLD** Locations Instrumented

Figure RAI 13-2: GKN1 Cycle 26 Map 32 Assembly F11 F_{dh} Pin Axial Distributions

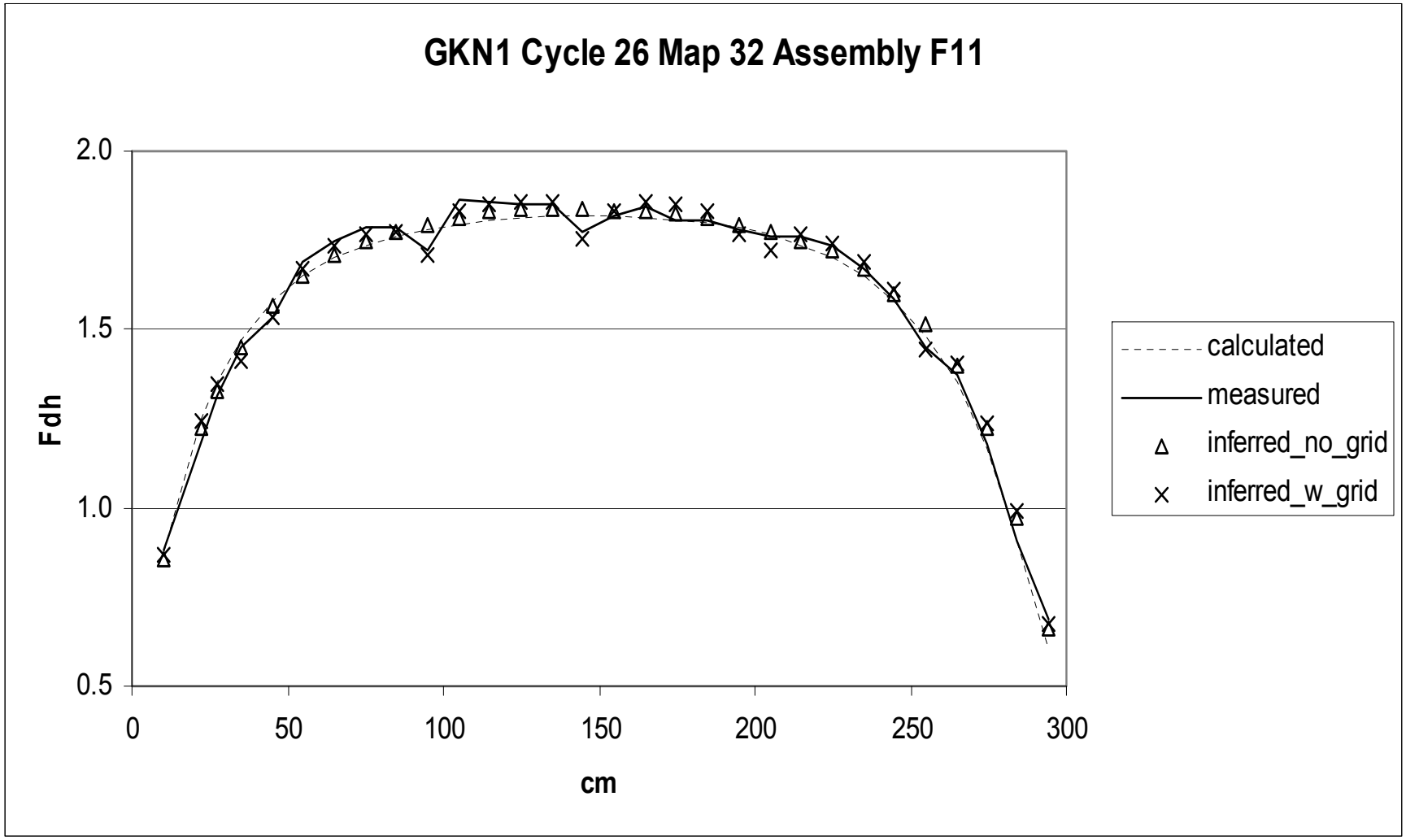

RAI-14. *Provide measured data to support local peaking factor uncertainty discussed in Section E.7.4 of ANP-10287 over the relevant range of exposures where a fuel pin would be limiting.*

Response 14:

The method used to determine the total peaking uncertainty is summarized below. CASMO3 calculations are used to illustrate the local and global nature of activation rate and peaking factor predictions. Measured to predicted activation rates, as a function of burnup, are used to demonstrate the applicability of the uncertainty method over the relevant range of exposures where a fuel pin would be limiting.

The total peaking uncertainty is composed of two components of uncertainty, local and global. These two components are estimated with calculations and measurements and are assumed to be independent. The local uncertainty component is estimated using critical experiments. These types of critical experiments are only available with burnup free fuel designs and have been historically used and approved to validate local peaking uncertainties for PWR operations and methods. The use of these benchmarks has been approved in references for PRISM, MICROBURN-P, NEMO, SCIENCE, and PDQ.

The global uncertainty component is estimated by a comparison of assembly/nodal powers obtained with operable detectors and the same assembly/nodal powers obtained with each detector, individually, assumed inoperable. The total error is a statistical combination of the local and global uncertainties.

CASMO3 calculations are used to obtain local peaking factors as a function of burnup. These same calculations are also used to obtain conversion factors at the instrumented location in the assembly as a function of burnup. These factors are used in the conversion of the PRISM calculated powers to calculated activation rates in instrumented locations. The methodology can be illustrated with a combined group conversion factor calculated as follows:

$\frac{A^{n,c}}{\phi_{total}^{c}} = \frac{\sigma_1^n \phi_1^{n,d,c} + \sigma_2^n \phi_2^{n,d,c}}{\phi_1^{n,c} + \phi_2^{n,c}}$ = The ratio of the activation rate in the instrument tube to the total nodal flux.

Where:

$A^{n,c}$ = Calculated activation rate in node n

σ_g^n = Calculated absorption cross section of the detector in group g for the fuel type and burnup in node n

$\phi_g^{n,d,c}$ = Calculated local flux at the location of the detector in group g for the fuel type and burnup in node n

$\phi_g^{n,c}$ = Calculated flux in group g for the fuel type and burnup in node n

As with the local peaking factors, conversion factors are for a specific location in the assembly. Comparisons of conversion factors from guide tube locations which are within three pin cells from the actual detector location can be used to simulate the local variation that is occurring.

Conversion factors were generated as a function of burnup and instrumented location for two fresh assemblies from GKN2 Cycle 5. The assembly layout for the GKN2 18 x 18 assembly types is shown in Figure RAI 14-1.

Assuming octant symmetry and a non-gad assembly, there are four locations which could be considered for the instrumented location. In Figure RAI 14-1 the four instrumented locations are denoted with a superscript (i.e., A, B, C, and D). Location A is the current location used in GKN2 for the instrumented location.

For two assembly types, CASMO3 was depleted to 80 GWd/MTU. At multiple burnup steps calculations were performed placing the instrument tube in each of the four locations. Results for locations B, C, and D were compared to the results for location A.

- The first assembly type was a non-gad assembly with 3.80 without U235 enrichment. The percent differences between the calibration factor results are presented in Figure RAI 14-2.

- The second assembly was a gad assembly with 3.80 without U235 enrichment and twelve pins of seven without gad at 2.60 without U235 enrichment. The gad rod locations are shown in Figure RAI 14-1. For locations C and D in the gad assembly, gad rods are located diagonally adjacent to the instrumented location. The results are presented in Figure RAI 14-3.

Figure RAI 14-2 shows a spread of over 4% is observed for the non-gad assembly, and Figure RAI 14-3 shows a similar spread after the gadolinia burns out.

The results in Figures RAI 14-2 and 14-3 are generated in an infinite assembly environment. To analyze the sensitivity of the detector locations in the presence of burnup gradients (global effect), 2 x 2 colorset calculations (colorset calculations are 2x2 arrays of assemblies) were performed. The following two burnup distributions were analyzed using periodic boundary conditions and the detector responses in the lower left assembly (0.1 GWd/MTU) were analyzed:

GWd/MTU

Distribution 1	
15	32
0.1	15

Distribution 2	
15	15
0.1	32

For the non-gad assembly all four detector locations were studied.

Non-Gad Assembly % Difference from Location A

Distribution 1		
B vs A	C vs A	D vs A
4.38	5.29	-2.14

Distribution 2		
B vs A	C vs A	D vs A
5.19	6.94	-0.46

For the gad assembly only locations A and B were studied (Note that at 0 GWd/MTU the difference was approximately 0 % for the infinite assembly solution).

Gad Assembly % Difference Location B versus A

Distribution 1	Distribution 2
1.63	2.50

As seen from these results, in the presence of burnup gradients, the sensitivity of the conversion factors to the instrumented location can be much larger. This illustrates the ability of the detector to sense local variations in power distributions from both an inter-assembly (global effect) and an intra-assembly basis (local effect). This demonstrates that the global uncertainty contribution to the total uncertainty includes an additional local uncertainty component, which is conservative.

Using the GKN1 and GKN2 database used for the uncertainty analysis, calculated activation rates were compared to measured activation rates at each measured location for fresh and once-burnt assemblies.

Figure RAI 14-4 illustrates the behavior of the calculated versus measured activation rates versus burnup up to 35 GWd/MTU, well above where assemblies are expected to be limiting. The x-axis is assembly average burnup. No degradation with burnup is observed.

Therefore, the method of using local uncertainties from the critical experiments and combining with the global power uncertainty to obtain a total uncertainty is applicable for pin power peaking over the range of burnups where a pin is expected to be limiting.

Figure RAI 14-1: GKN2 Assembly Guide Tube Configuration

3	3	3	3	3	3	3	3	3	3	3	3	3	3	3	3	3	3
3	3	3	3	3	3	3	3	3	3	3	3	3	3	3	3	3	3
3	3	**4**	3	3	3	1	3	3	3	3	1	3	3	3	**4**	3	3
3	3	3	1	3	3	3	3	3	**4**	3	3	3	3	1	3	3	3
3	3	3	3	**4**	3	3	1	3	3	1	3	3	**4**	3	3	3	3
3	3	3	3	3	1	3	3	3	3	3	3	1	3	3	3	3	3
3	3	1	3	3	3	3	3	3	3	3	3	3	3	3	1	3	3
3	3	3	3	1	3	3	3	3	3	3	3	3	1	3	3	3	3
3	3	3	**4**	3	3	3	3	3	3	3	3	3	3	3	3	3	3
3	3	3	3	3	3	3	3	3	3	3	3	3	3	**4**	3	3	3
3	3	3	3	1	3	3	3	3	3	3	3	3	1	3	3	3	3
3	3	1	3	3	3	3	3	3	3	3	3	3	3	3	1	3	3
3	3	3	3	3	1	3	3	3	3	3	3	1[C]	3	3	3	3	3
3	3	3	3	**4**	3	3	1	3	3	1[B]	3	3	**4**	3	3	3	3
3	3	3	1	3	3	3	3	**4**	3	3	3	3	3	1[D]	3	3	3
3	3	**4**	3	3	3	1	3	3	3	3	2[A]	3	3	3	**4**	3	3
3	3	3	3	3	3	3	3	3	3	3	3	3	3	3	3	3	3
3	3	3	3	3	3	3	3	3	3	3	3	3	3	3	3	3	3

1	Guide tube location
2	Guide tube with instrument
3	UO_2 Rod
4	UO_2 Rod or Gad Rod

Figure RAI 14-2: GKN2 Assembly Type 1 Conversion Factor Sensitivity to Instrumented Location

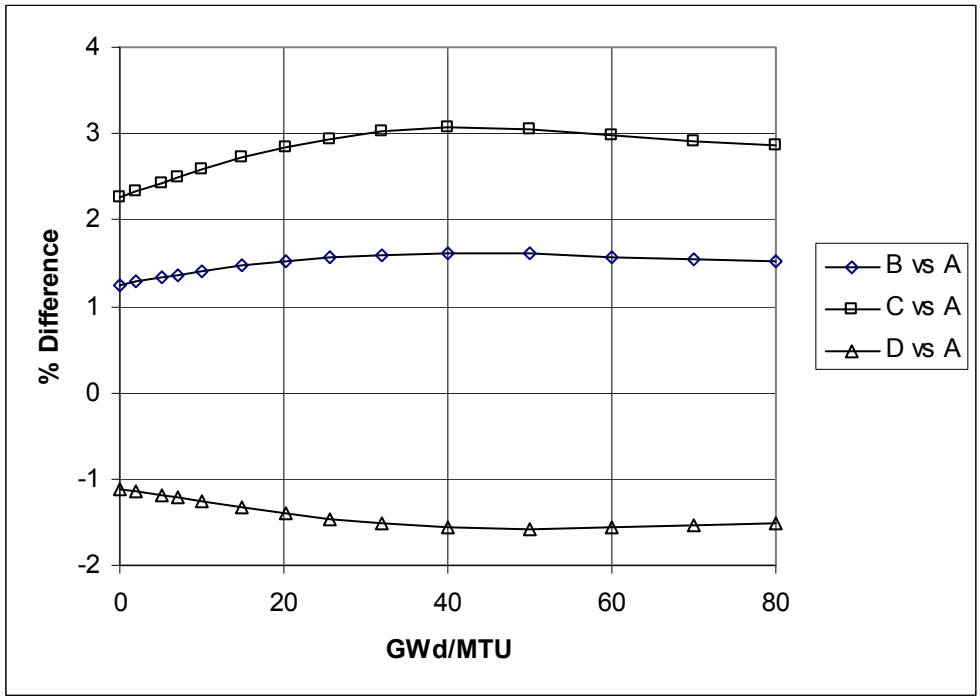

Figure RAI 14-3: GKN2 Assembly Type 2 Conversion Factor Sensitivity to Instrumented Location

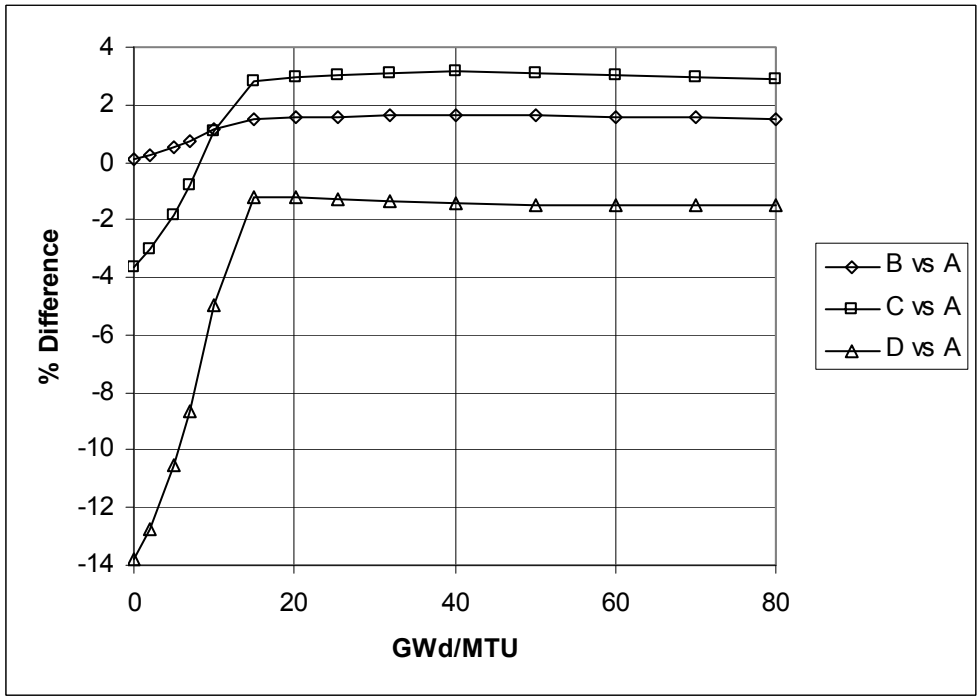

Figure RAI 14-4: GKN 1/2 Calculated Versus Measured Activation Rates